Biomineralization

International Edition: DOI: 10.1002/anie.201508010
German Edition: DOI: 10.1002/ange.201508010

Direct Observation of the Distribution of Gelatin in Calcium Carbonate Crystals by Super-Resolution Fluorescence Microscopy

Meifang Fu, Anhe Wang, Xiaoming Zhang, Luru Dai, and Junbai Li**

Abstract: *Biological organic–inorganic hybrid materials often achieve excellent properties and provide inspiration for the design of advanced materials. The organic phase plays a key role in determining the properties of biogenic materials, and the spatial arrangement of organic and inorganic phases provides direct evidence for interaction between the two phases. Super-resolution fluorescence microscopy was used to visualize the gelatin distribution in two different crystalline polymorphs of calcium carbonate (vaterite and calcite) and to investigate the process by which gelatin is excluded from the crystals. The results demonstrated that gelatin is distributed through vaterite microspheres in the form of nanoparticles, whereas it tends to accumulate on the edges of the calcite rhombohedra.*

Biominerals such as bone, teeth, and seashells are biological organic–inorganic hybrid materials[1–3] and often achieve extraordinary physical properties.[4–6] In order to design materials with advanced properties, many efforts have been spent in elucidating the functions of the organic component, which include induced nucleation,[7] stabilization of crystalline polymorphs,[8–10] and control of crystal morphology.[11–14] In all these aspects, the spatial distribution of organic and inorganic phases provides direct evidence for the interaction of the two phases and correlates with the gross morphology of the biogenic crystal.[15] Biomineralization is a dynamic process and proteins control the whole process of crystal nucleation, crystal growth, and phase transformation.[16,17] Direct observation of the dynamic association of the organic and inorganic phases will give us more in-depth information about the mechanism of biomineralization.

Fluorescence imaging enables direct observation when the organic phase is labeled with fluorescent dyes. However, some synthetic[18,19] and biological[12,20] materials contain nanoscale structures that are beyond the resolving power of traditional wide-field optical microscopy. Electron microscopy (EM) can achieve high spatial resolution but lacks molecular specificity. Moreover, it is difficult for EM to provide dynamic information directly. The development of super-resolution microscopy may help resolve this problem. The nanoscale resolution of super-resolution microscopy is especially suitable for nondestructively detecting dynamic process in nanostructures. Among super-resolution microscopy techniques, (direct) stochastic optical reconstruction microscopy ((d)STORM), which is based on detection and localization of the signal of a single fluorescent molecule, can achieve 20–30 nm lateral resolution.[21,22] This technique has been widely used in cell biology,[23] for example, in distinguishing the nanoscale structures in cell compartments like the nucleus[24] and cell organelles,[25] or acquiring the distributions of proteins on cell membranes.[26,27]

In our study, dSTORM was applied to detect the distribution of gelatin in two different crystalline polymorphs of synthetic calcium carbonate (vaterite and calcite). Calcium carbonate is the most abundant biomineral and plays an important role both in nature and industrial applications.[28] Gelatin, which is the partial degradation product of collagen, is widely used to study the role of protein networks in the formation of biominerals in vitro.[29] As far as we know, this is the first time dSTORM has been applied to the field of biomineralization.

Gelatin was labeled with a Cy5 NHS ester through an amide bond and vaterite microspheres with gelatin were prepared through one-step protein/$CaCO_3$ co-precipitation.[30] Scanning electron microscopy (SEM; Figure 1 a,b) and transmission electron microscopy (TEM; Figure 1 e) images reveal the rough surface of the fabricated vaterite microspheres.

Unlike the homogeneous distribution of silk fibroin (SF) in vaterite shown by element mapping,[31] the dSTORM images (Figure 1 d) showed that gelatin is distributed through vaterite microspheres in a form of nanoparticles. It has been shown that vaterite fabricated with[31] or without[32] additives consists of nanoparticles with similar dimensions to the first formed nanoparticulate amorphous calcium carbonate (ACC). The zeta potential of gelatin is −13.2 mV and it could thus interact with Ca^{2+} to form a gelatin–Ca complex that acts as a nucleation agent. Gelatin–$CaCO_3$ nanoparticles then form and aggregate to form the vaterite microspheres. The gelatin distribution thus reveals the formation mechanism of vaterite microspheres.

If the vaterite microspheres were opaque, we would only have been able to get a ring shape through optical sectioning. The distribution of gelatin was almost uniform in vaterite microspheres, however, so it can be deduced that the interior signal could pass through the vaterite microspheres and be received. The signals in the middle of the dSTORM image (Figure 1 d) reveal the gelatin distribution inside the micro-

[*] M. Fu, Prof. Dr. J. Li
Beijing National Laboratory for Molecular Sciences (BNLMS)
CAS Key Lab of Colloid, Interface and Thermodynamics
Institute of Chemistry, Chinese Academy of Sciences
100190 Beijing (China)
E-mail: jbli@iccas.ac.cn
Dr. A. Wang, Dr. X. Zhang, Prof. Dr. L. Dai
CAS Key Laboratory for Biomedical Effects of Nanomaterials and Nanosafety, National Center for Nanoscience and Technology
100190 Beijing (China)
E-mail: dai@nanoctr.cn

Supporting information for this article is available on the WWW under http://dx.doi.org/10.1002/anie.201508010.

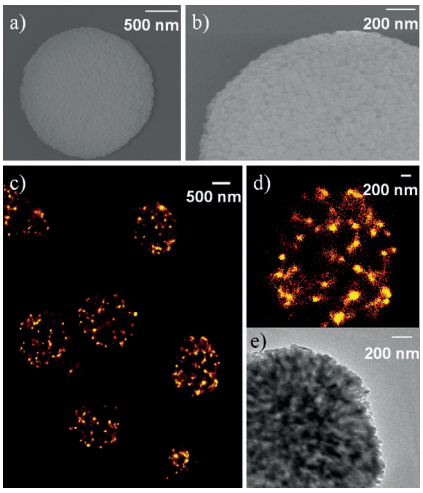

Figure 1. Nanostructures of fabricated vaterite microspheres and the gelatin distribution within them. a) SEM image of a $CaCO_3$ microsphere produced with gelatin. b) Magnified section of (a). c) dSTORM image of gelatin in $CaCO_3$ microspheres. d) Magnified section of (c). e) TEM image of a $CaCO_3$ microsphere.

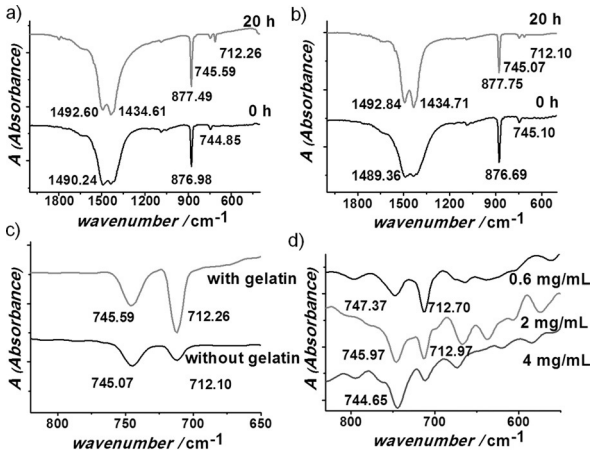

Figure 2. FTIR spectra of $CaCO_3$ produced with and without gelatin. a) FTIR spectra of $CaCO_3$ produced without gelatin measured just after centrifugation and after 20 h in water. b) FTIR spectra of $CaCO_3$ produced with gelatin measured just after centrifugation and after 20 h in water . c) Contrast FTIR spectra of $CaCO_3$ produced with and without gelatin after 20 h in water. d) IR spectra of $CaCO_3$ with different concentrations of gelatin. The $CaCO_3$ crystal was left in water for 4 h. The concentrations of gelatin were 0.6 mg mL^{-1}, 2 mg mL^{-1}, 4 mg mL^{-1}. The 713 cm^{-1} and 744 cm^{-1} peaks indicate calcite and vaterite, respectively

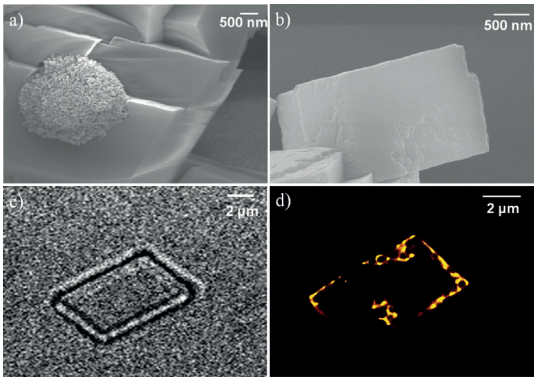

Figure 3. Structures of calcite rhombohedra and the distribution of gelatin within them. a) SEM image of the intermediate state of transformation from vaterite microspheres to calcite rhombohedra. b) SEM image of a calcite rhombohedron. c) Bright-field image of a calcite rhombohedron. d) dSTORM image of gelatin in a calcite rhombohedron.

sphere, whereas the signals on the edge of the image reveal gelatin distribution on the surface of the microsphere. So when we use dSTORM to observe the distributions of proteins in hybrid materials, whether or not the materials are transparent must be considered. If the material is not transparent, the signals from the interior of crystal cannot be received. In this case, one can image ultrathin sections of the material.

IR was used to analyze the effect of gelatin on the stabilization of vaterite. The proportion of absorptions at 712 cm^{-1} and 745 cm^{-1} reveal the relative content of calcite and vaterite phases in the fabricated $CaCO_3$ crystal.[33] The crystalline polymorphs of $CaCO_3$ obtained immediately after centrifugation were vaterite in both cases (Figure 2 a,b). After 20 h, however, vaterite microspheres with gelatin transformed into calcite in a higher proportion (Figure 2 c). However, the vaterite phase was stable for a longer time with increased concentrations of gelatin (Figure 2 d). So gelatin promotes the transformation of vaterite at low concentrations and stabilizes the vaterite phase at higher concentrations.

It has been found that some additives[31,34,35] can stabilize vaterite in a concentration-dependent manner due to surface adsorption. This helps explain the effect of gelatin on the stabilization of vaterite. At low concentrations, most of the gelatin is incorporated into vaterite microspheres and there is little adsorption of gelatin on the surface. Moreover, gelatin is an amphoteric electrolyte and cannot associate with Ca^{2+} as tightly as polyanions. With increased concentrations of gelatin, the adsorption of gelatin on the surface of vaterite microspheres will increase and the diffusion of Ca^{2+} and CO_3^{2-} is restricted, thus hindering the transformation of vaterite into calcite.

Overnight in water, vaterite microspheres transformed into calcite rhombohedra (Figure 3 b) via an intermediate state (Figure 3 a). It is worth noting that the space between $CaCO_3$ nanoparticles in the intermediate state is larger than in the intact vaterite microspheres (Figure 1 a, b). This might be because water permeates into the vaterite microspheres and reduces their density.

The distribution of gelatin (Figure 3 d) in calcite rhombohedra (Figure 3 c) was very different to that in vaterite microspheres. The gelatin was mostly distributed on the edge of the calcite rhombohedra in a continuous manner, with a small amount of gelatin located in the interior of the rhombohedra like small islands. During the transformation, the vaterite microspheres dissolve to release calcium and carbonate ions into solution and a calcite phase forms on the surface of vaterite microspheres. Since the solubility of calcite is lower than that of vaterite,[36] water cannot enter the

vaterite phase as easily once the calcite phase forms and the dissolution of the vaterite phase is thus restricted. Slow transformation leads to complete phase transformation of the contents inside the vaterite microspheres, leaving the characteristic spherical shape of vaterite intact.[31,32] The confined environment also restricts the expulsion of gelatin into the solution, thus resulting in gelatin islands on the surface of calcite rhombohedron.

During the transformation of vaterite into calcite, gelatin is excluded from the $CaCO_3$ crystal (Figure 4). The bright-field images of the sample (Figure S1 in the Supporting Information) show neither microspheres nor rhombohedra. The $CaCO_3$ crystals are thus in the intermediate state and consist of both calcite and vaterite phases. Although the bright-field images do not show big change during the imaging process, gelatin tends to accumulate on the edge of the crystals. The gelatin is hard to see in the last picture, which might be the result of either fluorescence quenching or complete removal of gelatin from the crystal. To address this, $CaCO_3$ stored in water for 5 days was imaged. The results showed that gelatin can still be seen on the edge of the rhombohedron and has a similar distribution to that seen in Figure 3d. So the apparent disappearance of gelatin is mainly because of fluorescence quenching. The reason that gelatin could not be completely excluded from the $CaCO_3$ crystal might be that gelatin does not dissolve in cold water and the $CaCO_3$ crystal can adsorb gelatin.

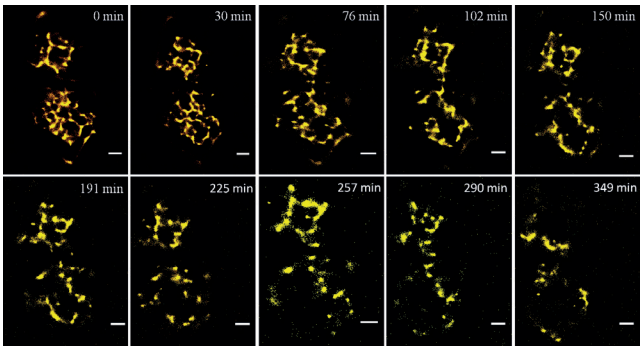

Figure 4. dSTORM images of the distributions of gelatin in $CaCO_3$ over time in switch buffer. Scale bar: 1 μm.

Aizenberg et al. have shown that fluorescent molecules can be removed from the growing crystal and accumulate at the framework–mineral interfaces.[37] It was expected that during the crystallization of ACC, the stabilizing macromolecules could also be excluded from the crystal.[13] The result that gelatin was excluded from $CaCO_3$ crystals proves that macromolecules can be excluded from the crystals during the transformation from vaterite into calcite. The dynamic distribution of gelatin may shed light on the dynamic interaction between macromolecules and biominerals. For example, it was found that defective distribution in immature sea urchin spines was much more isotropic than in mature spines.[15] Revealing the dynamic distribution of the defect will deepen our understanding of the different mechanisms of control in the two stages of biological crystal growth during spine formation. However, it is still a challenge to detect the dynamic distribution of macromolecules in biominerals in vivo. The difficulties come from fluorescent labeling of biological macromolecules, simulation of the biological environment when the imaging requires a particular buffer, and the limitation that dSTORM can only be used for surface detection when the crystal is opaque.

To conclude, we have demonstrated the extended application of dSTORM in the field of biomineralization. The distribution of gelatin in vateite microspheres is in the form of nanoparticles, which reflects the formation mechanism of vaterite microspheres with gelatin. In contrast, gelatin tended to accumulate on the edge of calcite rhombohedra. We were also able to show how gelatin is excluded from the $CaCO_3$ crystals during the transformation. Because the fluorescent labeling of proteins is simple, the method can be used to detect the distribution of numerous proteins in $CaCO_3$ with different morphologies. Furthermore, it can be extended to multicolor imaging to investigate the interaction between different proteins in synthetic and biological materials. Although the application of super-resolution microscopy to the field of biomineralization still faces many difficulties, the high resolution of this approach and its applicability to in situ testing will give us more distinct information about biomineralization from a new perspective.

Acknowledgements

The authors acknowledge the financial support from the National Natural Science Foundation of China (Project No. 21433010, 21320102004, 21321063, 21273053) and National Basic Research Program of China (973 program, 2013CB932802)

Keywords: biomimetic materials · calcium carbonate · hybrid materials · proteins · super-resolution microscopy

How to cite: *Angew. Chem. Int. Ed.* **2016**, *55*, 908–911
Angew. Chem. **2016**, *128*, 920–923

[1] F. Leroux, P. Rabu, N. A. J. M. Sommerdijk, A. Taubert, *Eur. J. Inorg. Chem.* **2015**, 1089–1095.
[2] K. Ariga, Q. M. Ji, M. J. McShane, Y. M. Lvov, A. Vinu, J. P. Hill, *Chem. Mater.* **2012**, *24*, 728–737.
[3] Y. Jia, J. B. Li, *Chem. Rev.* **2015**, *115*, 1597–1621.
[4] V. C. Sundar, A. D. Yablon, J. L. Grazul, M. Ilan, J. Aizenberg, *Nature* **2003**, *424*, 899–900.
[5] J. C. Weaver, G. W. Milliron, A. Miserez, K. Evans-Lutterodt, S. Herrera, I. Gallana, W. J. Mershon, B. Swanson, P. Zavattieri, E. DiMasi, D. Kisailus, *Science* **2012**, *336*, 1275–1280.
[6] S. Staniland, B. Ward, A. Harrison, G. van der Laan, N. Telling, *Proc. Natl. Acad. Sci. USA* **2007**, *104*, 19524–19528.
[7] J. M. Smeets, K. R. Cho, R. G. E. Kempen, N. A. J. M. Sommerdijk, J. J. D. Yoreo, *Nat. Mater.* **2015**, *14*, 394–399.
[8] J. Aizenberg, G. Lambert, L. Addadi, S. Weiner, *Adv. Mater.* **1996**, *8*, 222–226.
[9] C. Bassett, B. Marelli, S. N. Nazhat, J. E. Barralet, *Adv. Funct. Mater.* **2012**, *22*, 3460–3469.
[10] Y. U. Gong, C. E. Killian, I. C. Olson, N. P. Appathurai, A. L. Amasino, M. C. Martin, L. J. Holt, F. H. Wilt, P. U. Gilbert, *Proc. Natl. Acad. Sci. USA* **2012**, *109*, 6088–6093.

[11] O. E. Armitage, D. G. T. Strange, M. L. Oyen, *J. Mater. Res.* **2012**, *27*, 3157 – 3164.
[12] F. Nindiyasari, L. Fernández-Díaz, E. Griesshaber, J. M. Astilleros, N. Sánchez-Pastor, W. W. Schmahl, *Cryst. Growth Des.* **2014**, *14*, 1531 – 1542.
[13] N. A. J. M. Sommerdijk, G. de With, *Chem. Rev.* **2008**, *108*, 4499 – 4550.
[14] P. Simon, W. Carrillo-Cabrera, Y.-X. Huang, J. Buder, H. Borrmann, R. Cardoso-Gil, E. Rosseeva, Y. Yarin, T. Zahnert, R. Kniep, *Eur. J. Inorg. Chem.* **2011**, 5370 – 5377.
[15] J. Aizenberg, J. Hanson, T. F. Koetzle, S. Weiner, L. Addadi, *J. Am. Chem. Soc.* **1997**, *119*, 881 – 886.
[16] A. M. Belcher, X. H. Wu, R. J. Christensen, P. K. Hansma, G. D. Stucky, D. E. Morse, *Nature* **1996**, *381*, 56 – 58.
[17] E. Beniash, L. Addadi, S. Weiner, *J. Struct. Biol.* **1999**, *125*, 50 – 62.
[18] Y. Liu, Y. Cui, R. Guo, *Langmuir* **2012**, *28*, 6097 – 6105.
[19] K. Ariga, K. Kawakami, M. Ebara, Y. Kotsuchibashi, Q. M. Ji, J. P. Hill, *New J. Chem.* **2014**, *38*, 5149 – 5163.
[20] Y. Politi, R. A. Metzler, M. Abrecht, B. Gilbert, F. H. Wilt, I. Sagi, L. Addadi, S. Weiner, P. U. P. A. Gilbert, *Proc. Natl. Acad. Sci. USA* **2008**, *105*, 17362 – 17366.
[21] M. J. Rust, M. Bates, X. Zhuang, *Nat. Methods* **2006**, *3*, 793 – 795.
[22] M. Heilemann, S. van de Linde, M. Schuttpelz, R. Kasper, B. Seefeldt, A. Mukherjee, P. Tinnefeld, M. Sauer, *Angew. Chem. Int. Ed.* **2008**, *47*, 6172 – 6176; *Angew. Chem.* **2008**, *120*, 6266 – 6271.
[23] A. Oddone, I. V. Vilanova, J. Tam, M. Lakadamyali, *Microsc. Res. Tech.* **2014**, *77*, 502 – 509.
[24] A. Szymborska, A. de Marco, N. Daigle, V. C. Cordes, J. A. Briggs, J. Ellenberg, *Science* **2013**, *341*, 655 – 658.
[25] S.-H. Shim, C. Xia, G. Zhong, H. P. Babcock, J. C. Vaughan, B. Huang, X. Wang, C. Xu, G.-Q. Bi, X. Zhuang, *Proc. Natl. Acad. Sci. USA* **2012**, *109*, 13978 – 13983.
[26] C. G. Specht, I. Izeddin, P. C. Rodriguez, M. El Beheiry, P. Rostaing, X. Darzacq, M. Dahan, A. Triller, *Neuron* **2013**, *79*, 308 – 321.
[27] S. van de Linde, M. Sauer, M. Heilemann, *J. Struct. Biol.* **2008**, *164*, 250 – 254.
[28] X. Wang, R. Kong, X. Pan, H. Xu, D. Xia, H. Shan, J. R. Lu, *J. Phys. Chem. B* **2009**, *113*, 8975 – 8982.
[29] O. Grassmann, G. Müller, P. Löbmann, *Chem. Mater.* **2002**, *14*, 4530 – 4535.
[30] A. I. Petrov, D. V. Volodkin, G. B. Sukhorukov, *Biotechnol. Prog.* **2005**, *15*, 918 – 925.
[31] L. Liu, X. Zhang, X. Liu, J. Liu, G. Lu, D. L. Kaplan, H. Zhu, Q. Lu, *ACS Appl. Mater. Interfaces* **2015**, *7*, 1735 – 1745.
[32] J. D. Rodriguez-Blanco, S. Shaw, L. G. Benning, *Nanoscale* **2011**, *3*, 265 – 271.
[33] A. Cai, X. Xu, H. Pan, J. Tao, R. Liu, R. Tang, K. Cho, *J. Phys. Chem. C* **2008**, *112*, 11324 – 11330.
[34] J. Rieger, T. Frechen, G. Cox, W. Heckmann, C. Schmidt, J. Thieme, *Faraday Discuss.* **2007**, *136*, 265 – 277.
[35] Z. Zhang, D. Gao, H. Zhao, C. Xie, G. Guan, D. Wang, S. Yu, *J. Phys. Chem. B* **2006**, *110*, 8613 – 8618.
[36] L. N. Plummer, E. Busenberg, *Geochim. Cosmochim. Acta* **1982**, *46*, 1011 – 1040.
[37] J. Aizenberg, D. A. Muller, J. L. Grazul, D. R. Hamann, *Science* **2003**, *299*, 1205 – 1208.

Received: August 26, 2015
Revised: October 22, 2015
Published online: December 2, 2015

